Earthquake faults recorded in the near-shore bathymetry of Japan's back-arc

Luca C. Malatesta[1], Shigeru Sueoka[2], Nina-Marie Weiß[1], Boris Gailleton[3], Sumiko Tsukamoto[4,5], Daisuke Ishimura[6,7], Naoya Takahashi[8], Takuya Nishimura[9], Kyoko Kataoka[10], Tetsuya Komatsu[2], Yoshiya Iwasa[11]

[1]Earth Surface Process Modelling, GFZ Helmholtz Centre for Geosciences, Telegrafenberg, 14473 Potsdam, Germany
[2]Tono Geoscience Center, Japan Atomic Energy Agency, 509-5102 Toki, Japan
[3]Geosciences Rennes, University of Rennes, 35042 Rennes, France
[4]LIAG Institute for Applied Geophysics, Stilleweg 2, 30655 Hannover , Germany
[5]Department of Geosciences, University of Tübingen, Schnarrenbergstr. 94-96, 72076 Tübingen, Germany
[6]Department of Geography, Tokyo Metropolitan University, 192-0364 Hachioji, Japan
[7]Department of Earth Sciences, Chiba University, 263-8522 Chiba, Japan
[8]Department of Earth Sciences, Tohoku University, 980-8578 Sendai, Japan
[9]Disaster Prevention Research Institute, Kyoto University, 611-0011 Kyoto, Japan
[10]Research Institute for Natural Hazards and Disaster Recovery, Niigata University, 950-2181 Niigata, Japan
[11]Center for Education and Research of Disaster Risk Reduction and Redesign, Oita University, 870-1192 Oita, Japan

Key Points:

- The faults responsible for the 2024 M_W 7.5 Noto Peninsula Earthquake started their activity between 326 and 238 ka.
- The nearshore bathymetry of tectonically active coasts records changes in tectonic activity faster than the emerged landscape can adjust.
- The average position of the coastline over the last 100's kyr, at -60 m, is a useful marker to identify active faults at the edge of land.

Corresponding author: Luca C. Malatesta, `luca.malatesta@gfz.de`

Abstract

The eastern margin of the Sea of Japan is a zone of great seismic and tsunami hazard due to multiple offshore and nearshore reverse faults as shown by the 2024 M_W 7.5 Noto Peninsula Earthquake. Here we compare coseismic deformation of the 2024 Noto Peninsula Earthquake with 4767 individual marine terraces spanning the last Myr. This reveals that the earthquake faults started slipping between 326 and 238 ka. The emerged landscape is still adjusting to it while the nearshore domain already records it, in particular the -60 m trace of the average coastline across eustatic cycles. Applied to nearby Sado Island, these observations reveal the likely location of an active fault that drives its fast deformation. We show that scarps along the currently submerged "average coastline" are more likely to be active faults defining the edge of land.

Plain Language Summary

Earthquakes are a major source of risk for society, through the shaking, landslides, and tsunami they can generate. Along the northwest coast of Japan, it is difficult to identify which of the multiple of active tectonic faults, are more likely to cause violent earthquakes. On January First 2024, the M_W 7.5 Noto Peninsula earthquake ruptured along one of these faults, lifting land more than four meters at the coast. This event allows us to understand the relationship between its ground deformation and the landscape of the peninsula. We find that the repetition of a similar earthquakes every 2000 years for about 250'000 years can explain many features of the peninsula. More importantly, we identify a submarine ramp around 60 m below sea level at the location of the earthquake faults. 60 m depth is the average elevation of sea level over the last hundreds of thousand years. We propose here that in such coastal areas, the main earthquake faults are likely to be located offshore along that particular depth. This ramp at -60 m is an indicator of active earthquake faults and provides critical information about earthquake risk.

1 Introduction

1.1 The M_W 7.5 Noto Peninsula Earthquake in Japan's back-arc

Seismic hazards along Japan's back-arc are characterized by earthquakes up to M7 and M8 distributed on a large number of mostly offshore reverse faults (Earthquake Research Committee, 2024) uplifting inverted basins along the coast (Fig. 1) (Okamura et al., 1995). Through their shallow depths and close proximity to the coast, these faults produce strong surface shaking and short tsunami arrival times (Study Group on Research into Large-Scale Earthquakes in the Sea of Japan, 2016; Earthquake Research Committee, 2024). The Eurasia-North America boundary runs along the back-arc of the Japan subduction, either offshore or along the coast (Nakamura, 1983; Sagiya et al., 2000; Ohzono et al., 2011; T. Tamura et al., 2020) (Fig. 1 inset). The rarity of earthquakes on individual faults (Earthquake Research Committee, 2024) makes it hard to identify which of the many faults are most active.

On land, subaerial erosion reworks topography, inactive fault scarps progressively disappear and surface morphology is a good proxy for the degree of fault activity (Avouac & Peltzer, 1993). This sorting largely vanishes offshore where rates of erosion are extremely limited (Hughes et al., 2024). The nearshore domain is in an intermediate situation, eustatic cycles periodically expose the seafloor to wave and subaerial erosion in a gradient spanning ca. -120 m to modern sea level (Jara-Muñoz et al., 2017; Malatesta et al., 2021, 2022; Kluesner et al., 2023; Gowan et al., 2025). A better understanding of the bathymetric expression of active faults will provide insights into the earthquake cycle of the back-arc region.

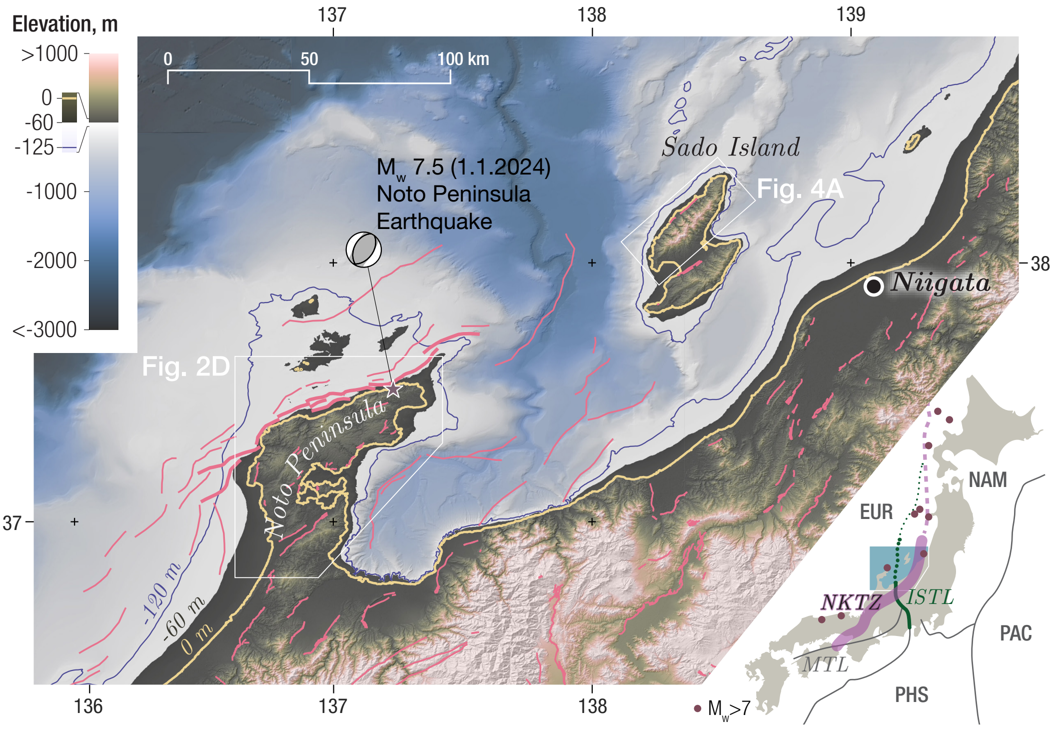

Figure 1. Regional map and tectonic context of the central coast of the Japan Sea with the Noto Peninsula and Sado Island with sea level at -60 m reflecting the average coastline over the last 100's kyr. Mapped active faults are marked in pink, thicker ones slipped in the Noto Peninsula Earthquake (Earthquake Research Committee, 2024). The -120 m low stand is traced as well (Gowan et al., 2025). Inset shows the main tectonic plates EURasia, North AMerica, PACific, PHilippine Sea; onshore lineaments of the Niigata-Kobe-Tectonic-Zone (Sagiya et al., 2000), Itoigawa-Shizuoka-Tectonic-Line, and Median-Tectonic-Line; $M_W > 7$ earthquakes along the Japan Sea coast since 1900. Bathymetry from Japan Hydrographic Association, topography from ASTER (ASTER Science Team, 2019).

On 1.1.2024, a M_W 7.5 earthquake shook the northern coast of the Noto Peninsula, on the back-arc side of Central Japan, at the eastern edge of the Eurasian plate (Fig. 1, 2 A–D) (Ma et al., 2024; Okuwaki et al., 2024; Yoshida et al., 2024; Fukushima et al., 2024). The quake ruptured multiple southeast-dipping reverse faults and capped a 36-month period of sustained swarm activity distributed on a set of parallel faults centered in northeast Noto and linked to migrating fluids (Nishimura et al., 2023; Yoshida et al., 2023; Kato, 2024). As of January 2025, the earthquake cost the lives of 515 persons and close to 150,000 structures were destroyed or damaged (Cabinet Office of Disaster Management in Japan, 2025). Several faults had failed individually ($M_W > 6$) over the last decades (Inoue et al., 2007; Ozawa et al., 2008; Awata et al., 2008; Hamada et al., 2016) but a combined rupture had not been observed in historical records. Three levels of Holocene marine terraces along the northwest coast of the peninsula suggest the recurrence of earthquakes with meter-scale throw at the coast (Shishikura et al., 2020).

At the surface, the Noto Peninsula Earthquake had a dramatic impact with a maximum 4.4 m of coastal uplift in the northwest. Up to 200 m wide bedrock platforms were lifted out of the water (Fig. 2 A–C) (Fukushima et al., 2024). If the emerged volcaniclastic platforms resist wave erosion, they will become new marine terraces, record the coseismic uplift, and act as passive strain markers (Otsuka, 1932; Yoshikawa, 1964; Ota

& Yoshikawa, 1978; Fukushima et al., 2024). Here, we use the complete marine terrace record to identify onset of deformation and the related nearshore scarps off the peninsula and nearby Sado Island.

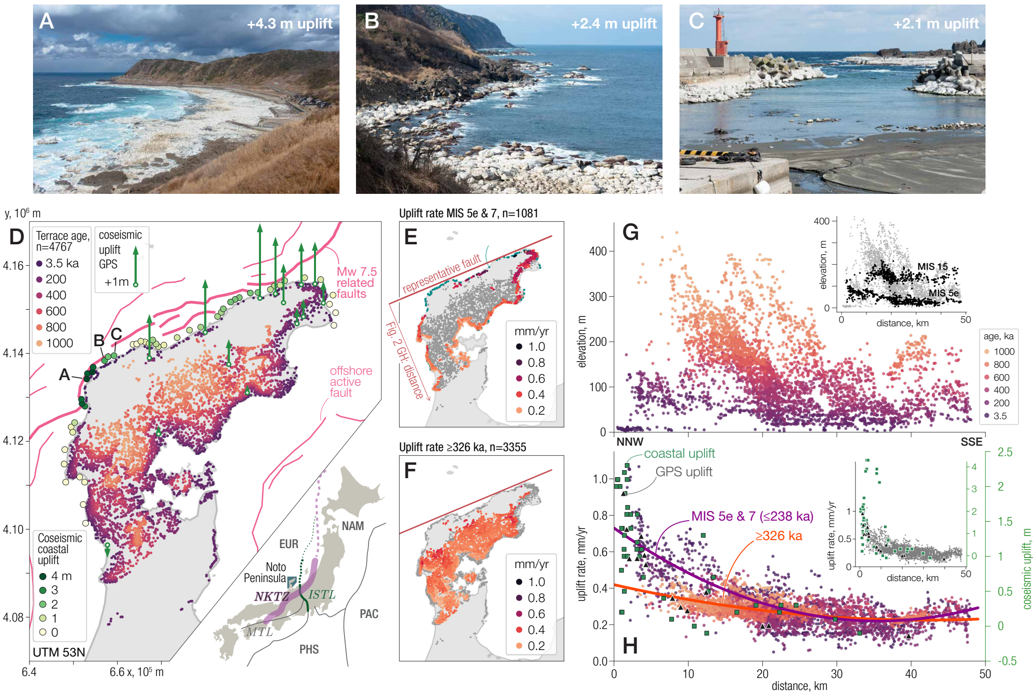

Figure 2. A–C: Coseismic uplift and coastal advance in Yoshiura, Kamiozawa, and Ozawa, March 2024. Tidal range is 0.4 m. D: Noto Peninsula with mapped active faults (Earthquake Research Committee, 2024), coseismic GPS deformation, coseismic uplift at the coast (Fukushima et al., 2024) and marine terraces (Koike & Machida, 2001; Ota & Hirakawa, 1979). E: Rock uplift rate from terraces of last two interglacial highstands, MIS 5e and 7 (121 and 238 ka) and position of Holocene terraces. F: Uplift rate from terraces MIS 9 (326 ka) and older. G: Elevation and age of all marine terraces as a distance away from the fault (see Fig. 1 E). Inset: same data highlighting tilt of MIS 5e terraces relative to MIS 15 (572 ka). H: Uplift rates derived from the marine terraces (MIS 5e and older)). Terraces older than 326 ka collapse on a relatively uniform rate of 0.3-0.4 mm/yr, while younger terraces (MIS 5e and 7) display a tilt that shares the same pattern as the coseismic deformation (Nishimura et al., 2024; Fukushima et al., 2024). Inset shows the entire scale for coastal survey. See Fig. S1 for a version using age on the x-axis and Fig. S2 for plots separating the two age groups.

2 Methods

We digitized 4767 unique terraces on the Noto Peninsula and 1019 on Sado Island from the Atlas of Quaternary Marine Terraces in the Japanese Islands (Koike & Machida, 2001; Ota & Hirakawa, 1979). We outlined each terrace of the Atlas on a more accurate 1 m DEM provided by the Ishikawa Prefecture, extracted the elevation of their highest boundary (the so-called paleo-shoreline angle), and recorded their coordinates and presumed age (data available in supplementary information). Then, Ota & Hirakawa (Ota & Hirakawa, 1979) had used the terraces as strain markers deviating from the horizontal sea level to identify a recent phase of faster uplift in the northwest (Fig. 2 G inset). We can now derive the rate of rock uplift for each terrace by calculating the ratio between the elevation gain from original sea level (Bintanja et al., 2005) to modern elevation and the age of the terrace (Fig. 2 G H). In the absence of documented shoreline markers, we rely on the necessary assumption that the terrace elevation corresponds to that of a past highstand. This might not always be the case (Malatesta et al., 2022) but the nearly continuous extent of individual terrace levels and the change in tilt of the terrace elevation alone strengthens this assumption.

We attribute a default age of 3.5 ka to Holocene terraces which are not radiometrically dated and do not use them for uplift rate calculations to avoid large uncertainties. In addition to the successive sea-level highstands, the Atlas attributes ages from the Marine Isotope Stage (MIS) 5a and 5c interstadials to terraces next to, and a few meters lower, than MIS 5e surfaces (Koike & Machida, 2001). The elevation difference between the interglacial and the subsequent interstadials is 35 and 37 m, respectively (Bintanja et al., 2005), resulting in a sharp increase in apparent rock uplift from MIS 5e to 5c and 5a. We prefer the interpretation of Ota and Hirakawa (1979) who attributed the MIS 5e age to their terrace *M1* based on fossil assemblages similar to those found on last interglacial surfaces elsewhere in Japan and who did not attribute specific interstadial ages to the associated lower levels of this surface (*M2* and *M3*). Rather, they call on unspecified periods of stillstand and transgression following the interglacial highstand. Near Suzu, the top deposits on the *M2* surface (interpreted as MIS 5c by Koike and Machida (2001)) cover shells associated with an *M1* age (i.e., MIS 5e) reflecting a reoccupation episode. We also exclude fast uplifting terraces on the topographic ridge to the southeast of the peninsula and the eastern part of Noto Island (central bay, Fig. 2 D) as they lies across a large active structure.

3 Results

3.1 Start of fault activity recorded by marine terraces

The Noto Peninsula hosts one of the longest and best mapped series of erosive marine terraces on the globe with 4767 unique terraces spanning the last million years (Fig. 2 D) (Koike & Machida, 2001; Ota & Hirakawa, 1979). They result from the combined action of rock uplift and wave erosion and can be cautiously interpreted as records of past sea level highstands (Yoshikawa, 1964; Anderson et al., 1999; Malatesta et al., 2022). The highest terraces are correlated to MIS 29, with an age of 1.02 Ma. Radiometric age and tephro-stratigraphic constraints for MIS 5e — the last Interglacial highstand — exist in the southeast of the peninsula (Omura, 1980). Older surfaces were only identified with a morphostratigraphic approach (Koike & Machida, 2001; Ota & Hirakawa, 1979). Terraces are extensively distributed on the southeastern half of the peninsula, while only Last Interglacial and Holocene terraces are found in the other half (Fig. 2 E, F). Coseismic uplift varies along the Noto coast and there are no MIS 5e marine terraces where it is highest (Fig. 2 D). But in the central northern coast, at the mouth of the Machino River (Fig. 3) a MIS 5e terrace lies at ca. 85 m elevation (Koike & Machida, 2001). Coseismic uplift was 1.7±0.05 m at the nearby site #38 of Fukushima et al. (2024). Factoring in 10% postseismic relaxation on that uplift value (Chen et al., 2024), we obtain a crude recurrence interval estimate of around 2.2 kyr for earthquakes of similar throw.

The elevation, age, and contemporary sea level of the marine terraces provide rock uplift rates across space and time (Fig. 2). Two trends emerge once terrace-derived uplift rate is plotted against the distance from the fault (Fig. 2 G, H). Terraces of the most recent two interglacials (MIS 5e and 7) display a strong tilt, from up to ca. 1 mm/yr at the highest MIS 5e terraces to an average of 0.25±0.08 mm/yr further than 20 km from the active faults. This trend has a similar wavelength to the GPS record and coastal survey of coseismic displacement (Fig. 2 H). Holocene terraces also indicate recent episodes of rock uplift along the northwest coast (Fig. 2 E) (Shishikura et al., 2020). In contrast, terraces MIS 9 (326 ka) and older all collapse around a uniform rate of uplift of mean value 0.28 ± 0.06 mm/yr. A change in deformation mode between MIS 7 and 9 minimizes the root mean square error of the trends in rock uplift between older and younger terraces (Fig. S3).

The peninsula is segmented by secondary faults that offset the elevation of some terraces by up to tens of meters, adding scatter without obscuring dominant trends (Fig. 2) (Ota & Hirakawa, 1979). For example, the northwestern block of the peninsula moved independently by a few cm during the M_W 7.5 Noto Peninsula Earthquake (Fukushima et al., 2024). Given the dominance of the tilting signal, the fact that we do not accurately measure strain rates owing to the lack of radiometric dating, and that we only aim to identify when the main mode of deformation shifted, we considered the peninsula as a single block and ignored motion across the sub-blocks.

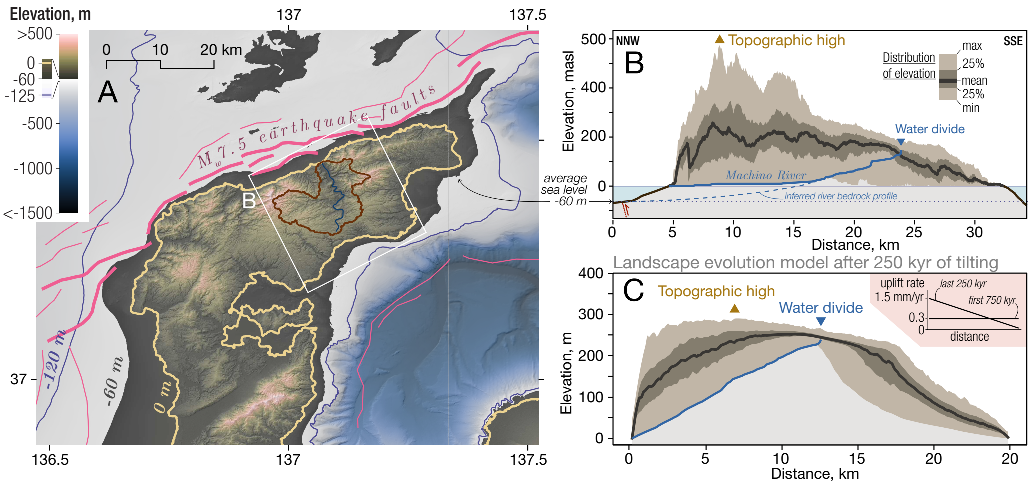

Figure 3. A: Map of Noto at average sea level of -60 m. The blue and yellow contours mark the last lowstand and current highstand. Offshore active faults are marked in pink (Earthquake Research Committee, 2024). The average coastline tracks many of the active faults that ruptured during the M_W 7.5 earthquake in Noto (thicker pink lines). B: 20 km-wide topographic swath profile across the Peninsula with the projected profile of the Machino River highlighting mismatch between drainage divide and high topography. C: Swath profile across a synthetic numerical landscape adjusting to tilting uplift. The mismatch of drainage divide and topographic high is replicated, see Fig. S5 for more details. Bathymetry from Japan Hydrographic Association, topography from ASTER (ASTER Science Team, 2019).

3.2 Transient landscape response

The modern coastline reflects a short-lived interglacial marine highstand. During the Last Glacial Maximum, sea level dropped to -120 m in the Sea of Japan (Gowan et al., 2025), but over the last half million years, its average elevation was around -60 m (Bintanja et al., 2005) (Fig. S4). Several of the many active reverse faults that ruptured on Jan. 1st 2024 follow this average coastline (Fig. 3 A) (Inoue et al., 2007; Inoue & Okamura, 2010). The colocation suggests that fault activity has set the base level for the peninsula long enough to anchor the average position of its coastline. A fault that marks the edge of land uplift should intuitively be located offshore during highstands, at the limit of the domain that is more often emerged than drowned. Using the average coastline instead of the modern highstand coastline reveals dominant features in a tectonically active landscape.

Contrary to the average coastline matching the active faults, the fluvial landscape of the peninsula is not equilibrated to a faster uplift rate in the north (Fig. 3). In the Machino River catchment, largest of the peninsula, the highest point (544 m) is found in the north, away from the main water divide to the south (Fig. 3 B). The Machino catchment occupies nearly 90% of the width of the peninsula and reaches the sea flowing across a wide alluvial plain. This geometry is in apparent contradiction with a field of rock uplift rate increasing to the north. At equilibrium this would call for shorter and steeper catchments to the north while the southern catchments would be gentler and longer as is the case, e.g., in Sicily (Pavano & Gallen, 2021).

This paradox can be solved considering two important points: 1) the strong tilting is a geologically recent event and the landscape currently adjusts to it, and 2) the Noto Peninsula has inherited an asymmetric topography as it emerged from the sea. The tilting of marine terraces 238 ka and younger supports the first point. The bathymetry and topography of the Noto Peninsula is strongly asymmetric with a steep southern flank and a very gentle northern flank (Fig. 1). The previously uniform and steady uplift rate recorded by older terraces would lead to initially steep and short catchments to the south due to the inherited submarine topography (Okamura et al., 1995).

A simplified landscape evolution model (Gailleton et al., 2024) of the peninsula emerging from the sea shows how a 250 ka change from uniform to tilting uplift fields offsets the highest topography from the drainage divide during the transient response (Fig. 3 C, Fig. S5, supplementary information). The initial emerging landscape starts with a strong asymmetry reflecting a typical inverted basin (Okamura et al., 1995). Large catchments develop on the gentler left flank in the model. Once the uniform uplift field shifts to a tilting pattern, larger catchments can maintain a passage across the zone of faster uplift having already accumulated a large drainage area. This allows the main valleys to keep up with increased rock uplift rate, while the interfluves steepen. Rapidly, the topographic high migrates north, while the drainage divide remains south, a characteristic feature of the Noto Peninsula.

4 Discussion

4.1 Regional tectonic context

The onset of slip on Noto Peninsula's northern reverse faults between 326 and 238 ka (Fig. 2) is a recent tectonic evolution. The peninsula is marked by northeast striking reverse faults associated with back-arc deformation (Ishiyama et al., 2017). They are inherited from the back-arc opening from 25 to 13 Ma; after a 9.5 Myr period of neutral stresses, compression started at around 3.5 Ma (Sato, 1994). Reverse slip on the normal faults uplifted asymmetric inverted basins (Okamura et al., 1995). Most active reverse faults in Noto are located just offshore of its northern coastline (Fig. 1) (Inoue & Okamura, 2010). Another fault system, dipping northwest, flanks the peninsula to the south on the bottom of Toyama Bay at ca. 1 km depth (Ishiyama et al., 2017). This system could have contributed to the uniform and steady uplift rate recorded prior to the transfer on the northwest faults and contributed to the kilometer-deep relief between the peninsula and the floor of the bay. A similar transfer of slip from one reverse fault to its antithetic counterpart has been proposed for the growth of the Ou Backbone range of the Japan arc (Nakajima et al., 2006).

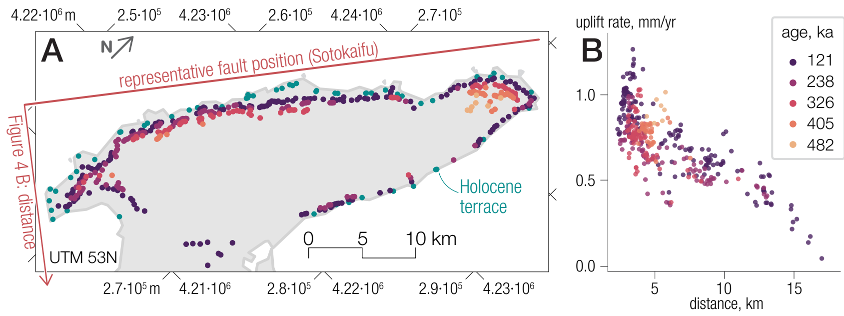

Figure 4. A: Location and age of marine terraces on Oosado (A. Tamura, 1979; Ota et al., 1992; Koike & Machida, 2001). The marker colors are shared across the subplots and indicated in B. The representative position of the Sotokaifu offshore fault is placed according to Ota et al. (1992). B: Uplift rates on Oosado as a function of distance from the proposed offshore Sotokaifu fault.

4.2 Application to the neighboring Sado Island

The relationship between landscape and seismicity exposed in the Noto Peninsula sheds light on the nearby Sado Island (Fig. 1), where data about the earthquake cycle is scant. Sado Island marks the southwestern end of the Sado Ridge(Okamura et al., 1995). Similar to the Noto Peninsula, a pattern of strong tilting to the southeast is recorded by MIS 7 and 5e terraces on Oosado, the northern range of Sado Island (Fig. 4, Fig. S6). The island is smaller, steeper, and higher (1172 m) than the Noto Peninsula and does not have an equivalent record of older terraces (Ôta, 1964). The MIS 9–13 marine terraces are too tightly clustered at both tips of Oosado to reveal a spatial pattern of uplift (Fig. 4).

Ota et al. (1992) noted the paradox of Last Interglacial marine terraces recording a strong tilt to the southeast while the landscape of Oosado has steeper, shorter, catchments to the southeast, with evidence of stream capture and divide migration towards the northwest (Sakashita & Endo, 2023). The steeper catchments could result from past activity on the northwest-dipping reverse fault that flanks the southeastern coast. That fault belongs to the series of reactivated normal faults that built the Sado Ridge since the Pliocene (Okamura et al., 1995; Watanabe et al., 1994). Ota et al. (1976, 1992) explain the recent tilting, as well as an onshore splay fault, by the activation of reverse thrusts “sometime before 300 ka” just offshore of the northwest coast of Oosado: the Sotokaifu Fault system. Due to its proximity to the coast and shallow depth, it is not listed amongst the large offshore earthquake faults (Study Group on Research into Large-Scale Earthquakes in the Sea of Japan, 2016; Okamura, 2019).

The nearshore Sotokaifu Fault System is too shallow for seismic surveys (Okamura, 2019) but bathymetry reveals similarities between Sado and Noto (Fig. 5). The position of the average -60 m coastline of Oosado is relatively straight, 1–3 km away from the modern highstand coastline (Fig. 5 B). The contour follows a scarp that resembles the one associated with the Noto Peninsula earthquake (Fig. 5 A). Its location is compatible with the main segment of the Sotokaifu Fault system proposed by Ota et al. (1992). Over 45 km long, the segment has a potential for $M \geq 7$ ruptures (Wells & Coppersmith, 1994). Based on the Noto Peninsula observations, we propose that the average coastline already records the position of the dominant fault system while the subaerial landscape is still adjusting to the new uplift pattern.

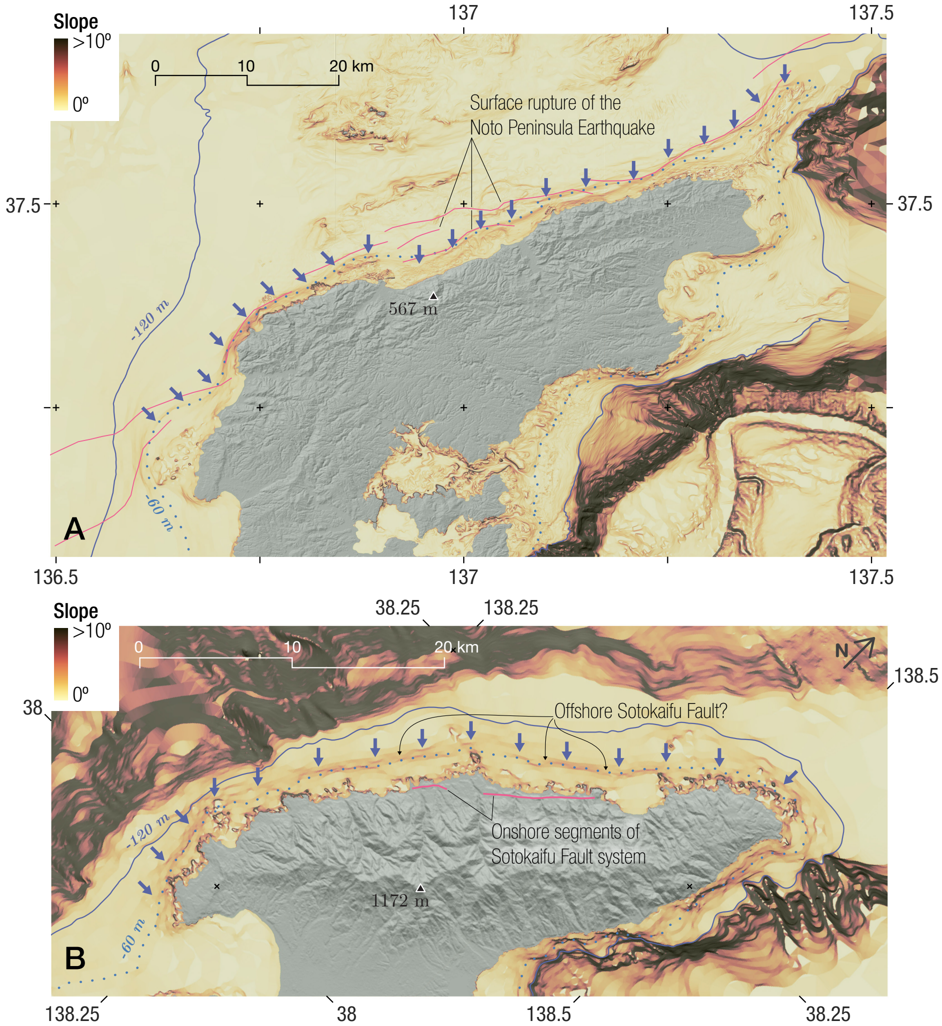

Figure 5. A and B: Offshore slope maps of Noto Peninsula and Oosado saturated at 10°. The solid line traces the -120 m low-stand contour, the dotted line marks the average -60 m coastline. The arrows point to the near continuous steeper scarp coinciding with the average coast. On the Noto Peninsula, this scarp matches the faults (thin pink lines) that ruptured during the 2024 Noto Peninsula Earthquake. Bathymetry from Japan Hydrographic Association, topography from ASTER (ASTER Science Team, 2019).

On Sado Island, the coseismic deformation resulting from a rupture similar to the Noto Peninsula Earthquake would cause significant uplift along the northwest coast and potential subsidence in the Kuninaka Plain to the southeast (see GPS in Fig. 2 D). Most of the population, agriculture and infrastructure of the island is located in the plain and coseismic subsidence would compound its tsunami exposure. A total 24 likely tsunami deposits over the last 9 kyr identified in the plain's lacustrine system confirm that risk (Urabe, 2017). A deposit (*KAM-Ev3*) dated at 1678–1781 CE is compatible with the 1762 CE M7 Horeki earthquake (Kawauchi, 2000). Villages in North Oosado were damaged by the tsunami of this event and its roughly estimated epicenter (Kawauchi, 2000) is broadly compatible with the Sotokaifu Fault system. The steep landscape of Oosado is also prone to landslides across critical roads (Shimizu & Oyagi, 1988) and the island already experienced liquefaction from the more distant 2024 Noto Peninsula Earthquake

(Cabinet Office of Disaster Management in Japan, 2025). The similarities in recent deformation and bathymetry with the Noto Peninsula and the faster uplift rates on Sado Island warrant attention to the risks it incurs.

4.3 Conclusion

The M_W 7.5 Noto Peninsula Earthquake of January First, 2024, provides unique information about the relationship between transient coastal landscapes and seismogenic faults characterized by long, often quiet, recurrence intervals. Repeated slip on the same fault system is responsible for the tectonic tilt on the peninsula since 324–238 ka following a previously uniform uplift. The ruptured faults are located offshore and most follow the trace of the average coastline over the last half million years at 60 m below sea level. Because the peninsula's subaerial landscape is not yet equilibrated to the new uplift gradient, the average coastline should be preferred to identify active faults. These observations can inform other sites where seismic information is limited. Nearby, the northern range of Sado Island, Oosado, shares the same pattern of recent tilting and transient landscape. Based on the Noto Peninsula, we propose that the offshore fault responsible for the tilting of Oosado can be found by tracing the average position of the coastline at -60 m. Given the on- and offshore similarities with the Noto Peninsula, we advise increased scrutiny of seismic hazards — shaking, tsunami, landslides, and liquefaction — on Sado Island.

Open Research Section

The dataset of terrace location, age, and elevation is available on the repository *WILL BE UPLOADED ON PUBLIC REPOSITORY AFTER PASSING REVIEW* and in the supplementary information of this article.

Acknowledgments

Discussions with J.-P. Avouac and A. Wickert helped shape this article. LCM and ST acknowledge are supported by a DFG individual Research Grant (no. 524080107).

References

Anderson, R. S., Densmore, A. L., & Ellis, M. A. (1999, March). The generation and degradation of marine terraces. *Basin Research*, *11*(1), 7–19. doi: 10.1046/j.1365-2117.1999.00085.x

ASTER Science Team. (2019). *ASTER Global Digital Elevation Model V003.* NASA EOSDIS Land Processes Distributed Active Archive Center. doi: 10.5067/ASTER/ASTGTM.003

Avouac, J.-P., & Peltzer, G. (1993). Active Tectonics in Southern-Xinjiang, China - Analysis of Terrace Riser and Normal-Fault Scarp Degradation Along the Hotan-Qira Fault System. *Journal of Geophysical Research*, *98*, 21773–21807.

Awata, Y., Toda, S., Kaneda, H., Azuma, T., Horikawa, H., Shishikura, M., & Echigo, T. (2008, October). Coastal deformation associated with the 2007 Noto Hanto earthquake, central Japan, estimated from uplifted and subsided intertidal organisms. *Earth, Planets and Space*, *60*(10), 1059–1062. doi: 10.1186/BF03352869

Bintanja, R., Van De Wal, R. S., & Oerlemans, J. (2005, September). Modelled atmospheric temperatures and global sea levels over the past million years. *Nature*, *437*(7055), 125–128. doi: 10.1038/nature03975

Cabinet Office of Disaster Management in Japan. (2025, January). *On the damages caused by the 2024 Noto Peninsula Earthquake (in Japanese)* (Tech. Rep.). Cabinet Office of Disaster Management in Japan.

Chen, Y., Li, J., Lu, K., & Hu, T. (2024, December). Coseismic slip model and early post-seismic deformation processes of the 2024 M7.5 Noto Peninsula, Japan earthquake revealed by InSAR and GPS observations. *Geophysical Journal International*, *240*(2), 1048–1063. doi: 10.1093/gji/ggae429

Earthquake Research Committee. (2024). *Long-term evaluation of the offshore active faults on the Japan Sea side: north of Hyogo prefecture to Joetsu region of Niigata prefecture (version August 2024, in Japanese)* (Tech. Rep.). Earthquake Research Committee.

Fukushima, Y., Ishimura, D., Takahashi, N., Iwasa, Y., Malatesta, L. C., Takahashi, T., ... Toda, S. (2024, December). Landscape changes caused by the 2024 Noto Peninsula earthquake in Japan. *Science Advances*, *10*(49), eadp9193. doi: 10.1126/sciadv.adp9193

Gailleton, B., Malatesta, L. C., Cordonnier, G., & Braun, J. (2024, January). CHONK 1.0: Landscape evolution framework: Cellular automata meets graph theory. *Geoscientific Model Development*, *17*(1), 71–90. doi: 10.5194/gmd-17-71-2024

Gowan, E. J., Tomita, T., Nishioka, D., Zhang, X., Sun, Y., Shi, X., ... Abe-Ouchi, A. (2025, February). Impact of topographic change on the East Asian monsoon in Japan and Eastern Asia during the Last Glacial Maximum. *Progress in Earth and Planetary Science*, *12*(1), 18. doi: 10.1186/s40645-024-00681-4

Hamada, M., Hiramatsu, Y., Oda, M., & Yamaguchi, H. (2016, February). Fossil tubeworms link coastal uplift of the northern Noto Peninsula to rupture of the Wajima-oki fault in AD 1729. *Tectonophysics*, *670*, 38–47. doi: 10.1016/j.tecto.2015.12.019

Hughes, A., Olive, J.-A., Malatesta, L. C., & Escartín, J. (2024, December). Characterization of bedrock mass-wasting at fault-bound abyssal hills. *Earth and Planetary Science Letters*, *648*, 119073. doi: 10.1016/j.epsl.2024.119073

Inoue, T., Murakami, F., Okamura, Y., & Ikehara, K. (2007). Offshore Active Faults in the Source Area of the 2007 Noto Hanto Earthquake (in Japanese). *Bulletin of the Earthquake Research Institute*, *82*(4), 301.

Inoue, T., & Okamura, Y. (2010). *1:200,000 Marine Geological Map around the Northern Part of Noto Peninsula.* Geological Survey of Japan, AIST.

Ishiyama, T., Sato, H., Kato, N., Koshiya, S., Abe, S., Shiraishi, K., & Matsubara, M. (2017, July). Structures and active tectonics of compressionally reactivated back-arc failed rift across the Toyama trough in the Sea of Japan, revealed by multiscale seismic profiling. *Tectonophysics*, *710–711*, 21–36. doi: 10.1016/j.tecto.2016.09.029

Jara-Muñoz, J., Melnick, D., Zambrano, P., Rietbrock, A., González, J., Argandoña, B., & Strecker, M. R. (2017, June). Quantifying offshore fore-arc deformation and splay-fault slip using drowned Pleistocene shorelines, Arauco Bay, Chile: Quantifying Offshore Deformation. *Journal of Geophysical Research: Solid Earth*, *122*(6), 4529–4558. doi: 10.1002/2016JB013339

Kato, A. (2024, January). Implications of Fault-Valve Behavior From Immediate Aftershocks Following the 2023 M_j 6.5 Earthquake Beneath the Noto Peninsula, Central Japan. *Geophysical Research Letters*, *51*(1), e2023GL106444. doi: 10.1029/2023GL106444

Kawauchi, K. (2000). Re-Examination of the Epicenter of the 1762 Horeki off Sado Earthquake (M7.0). *Rekishi Jishin*, *16*, 107–112.

Kluesner, J. W., Johnson, S. Y., Nishenko, S. P., Medri, E., Simms, A. R., Greene, H. G., ... Conrad, J. E. (2023, December). High-resolution geophysical and geochronological analysis of a relict shoreface deposit offshore central California: Implications for slip rate along the Hosgri fault. *Geosphere*, *19*(6), 1788–1811. doi: 10.1130/GES02657.1

Koike, K., & Machida, H. (2001). *Atlas of Quaternary Marine Terraces in the Japanese Islands.* Tokyo: University of Tokyo Press.

Ma, Z., Zeng, H., Luo, H., Liu, Z., Jiang, Y., Aoki, Y., ... Wei, S. (2024, July). Slow rupture in a fluid-rich fault zone initiated the 2024 M_w 7.5 Noto earthquake. *Science*, eado5143. doi: 10.1126/science.ado5143

Malatesta, L. C., Bruhat, L., Finnegan, N. J., & Olive, J.-A. L. (2021, January). Co-location of the Downdip End of Seismic Coupling and the Continental Shelf Break. *Journal of Geophysical Research: Solid Earth*, *126*(1). doi: 10.1029/2020JB019589

Malatesta, L. C., Finnegan, N. J., Huppert, K. L., & Carreño, E. I. (2022). The influence of rock uplift rate on the formation and preservation of individual marine terraces during multiple sea-level stands. *Geology*, *50*, 101–105. doi: 10.1130/G49245.1

Nakajima, T., Danhara, T., Iwano, H., & Chinzei, K. (2006, November). Uplift of the Ou Backbone Range in Northeast Japan at around 10 Ma and its implication for the tectonic evolution of the eastern margin of Asia. *Palaeogeography, Palaeoclimatology, Palaeoecology*, *241*(1), 28–48. doi: 10.1016/j.palaeo.2006.06.009

Nakamura, K. (1983). Possible Nascent Trench along the Eastern Japan Sea as the Convergent Boundary between Eurasian and North American Plates. *Bulletin of the Earthquake Research Institute*, *58*(3), 711–722. doi: 10.15083/0000032948

Nishimura, T., Hiramatsu, Y., & Ohta, Y. (2023, June). Episodic transient deformation revealed by the analysis of multiple GNSS networks in the Noto Peninsula, central Japan. *Scientific Reports*, *13*(1), 8381. doi: 10.1038/s41598-023-35459-z

Nishimura, T., Hiramatsu, Y., & Ohta, Y. (2024). Source models for the 2020-2024 Noto Peninsula earthquakes based on GNSS data. In *Abstracts of JpGU Meeting 2024* (p. U16-02). Chiba, Japan.

Ohzono, M., Sagiya, T., Hirahara, K., Hashimoto, M., Takeuchi, A., Hoso, Y., ... Doke, R. (2011, March). Strain accumulation process around the Atotsugawa fault system in the Niigata-Kobe Tectonic Zone, central Japan: Strain field around the Atotsugawa fault system. *Geophysical Journal International*, *184*(3), 977–990. doi: 10.1111/j.1365-246X.2010.04876.x

Okamura, Y. (2019, March). Distribution of Active Faults in Japan Sea and Future Issues. *Zisin (Journal of the Seismological Society of Japan. 2nd ser.)*, *71*(0), 185–199. doi: 10.4294/zisin.2017-21

Okamura, Y., Watanabe, M., Morijiri, R., & Satoh, M. (1995, September). Rifting and basin inversion in the eastern margin of the Japan Sea. *Island Arc*, *4*(3), 166–181. doi: 10.1111/j.1440-1738.1995.tb00141.x

Okuwaki, R., Yagi, Y., Murakami, A., & Fukahata, Y. (2024, June). A Multiplex Rupture Sequence Under Complex Fault Network Due To Preceding Earthquake Swarms During the 2024 Mw 7.5 Noto Peninsula, Japan, Earthquake. *Geophysical Research Letters*, *51*(11), e2024GL109224. doi: 10.1029/2024GL109224

Omura, A. (1980). 713. Uranium-series age of the Hirakodo and Uji shell beds, Noto Peninsula, Central Japan. *Transactions and proceedings of the Paleontological Society of Japan*, *117*, 247–253. doi: 10.14825/prpsj1951.1980.117_247

Ôta, Y. (1964). Coastal terraces of the Sado Island, Japan. *Geographical Review of Japan*, *37*(5), 226–242. doi: 10.4157/grj.37.226

Ota, Y., & Hirakawa, K. (1979). Marine terraces and their deformation in Noto Peninsula, Japan Sea side of Central Japan. *Geographical Review of Japan*, *52*(4), 169–189. doi: 10.4157/grj.52.169

Ota, Y., Matsuda, T., & Naganuma, K. (1976). Tilted Marine Terraces of the Ogi Peninsula, Sado Island, Central Japan, Related to the Ogi Earthquake of 1802. *Zisin (Journal of the Seismological Society of Japan. 2nd ser.)*, *29*(1), 55–70. doi: 10.4294/zisin1948.29.1_55

Ota, Y., Miyawaki, A., & Shiomi, M. (1992). Active Faults on Sado Island, off Central Japan, and Their Implication on the Marine Terrace Deformation. *Journal of Geography (Chigaku Zasshi)*, *101*(3), 205–224. doi: 10.5026/jgeography.101.205

Ota, Y., & Yoshikawa, T. (1978). Regional characteristics and their geodynamic implications of late quaternary tectonic movement deduced from deformed former shorelines in japan. *Journal of Physics of the Earth*, *26*(Supplement), S379-S389. doi: 10.4294/jpe1952.26.Supplement_S379

Otsuka, Y. (1932). Post Pliocene Crustal Movement in the Outer Zone of Southwest Japan and in the Fossa Magna. *Bulletin of the Earthquake Research Institute*, *10*(3), 701–722.

Ozawa, S., Yarai, H., Tobita, M., Une, H., & Nishimura, T. (2008, February). Crustal deformation associated with the Noto Hanto Earthquake in 2007 in Japan. *Earth, Planets and Space*, *60*(2), 95–98. doi: 10.1186/BF03352767

Pavano, F., & Gallen, S. F. (2021, July). A Geomorphic Examination of the Calabrian Forearc Translation. *Tectonics*, *40*(7), e2020TC006692. doi: 10.1029/2020TC006692

Sagiya, T., Miyazaki, S., & Tada, T. (2000). Continuous GPS Array and Present-day Crustal Deformation of Japan. *Pure appl. geophys.*, *157*.

Sakashita, A., & Endo, N. (2023, January). Mobility and Location of Drainage Divides Affected by Tilting Uplift in Sado Island, Japan. *Remote Sensing*, *15*(3), 729. doi: 10.3390/rs15030729

Sato, H. (1994, November). The relationship between Late Cenozoic tectonic events and stress field and basin development in northeast Japan. *Journal of Geophysical Research: Solid Earth*, *99*(B11), 22261–22274. doi: 10.1029/94JB00854

Shimizu, F., & Oyagi, N. (1988). *National Research Institute for Earth Science and Disaster Prevention, Landslide topography distribution map Volume 4 "Murakami and Sado"* (109th ed.). National Research Center for Disaster Prevention.

Shishikura, M., Echigo, T., & Namegaya, Y. (2020). Activity of the off-shore active faults along the northern coast of the Noto Peninsula deduced from the height distribution of the lower marine terrace and emerged sessile assemblage. *Active Fault Research*, *53*, 33–49.

Study Group on Research into Large-Scale Earthquakes in the Sea of Japan. (2016). *Report of the Study Group on Large-Scale Earthquakes in the Sea of Japan (in Japanese)* (Tech. Rep.). Ministry of Land, Infrastructure, Transport and Tourism.

Tamura, A. (1979). Holocene marine terraces and crustal movements of Sado Island, Central Japan. *Geographical Review of Japan*, *52*(7), 339–355. doi: 10.4157/grj.52.339

Tamura, T., Oohashi, K., Otsubo, M., Miyakawa, A., & Niwa, M. (2020, December). Contribution to crustal strain accumulation of minor faults: A case study across the Niigata–Kobe Tectonic Zone, Japan. *Earth, Planets and Space*, *72*(1), 7. doi: 10.1186/s40623-020-1132-5

Urabe, A. (2017, October). Reconstruction of tsunami history based on event deposits in the Niigata area, eastern coast of the Sea of Japan. *Quaternary International*, *456*, 53–68. doi: 10.1016/j.quaint.2017.05.045

Watanabe, M., Okamura, Y., & Satoh, M. (1994). Diatom fossil and geologic structure of the southeastern margin (off Tohoku) of the Japan Sea. *Bulletin of Geological Survey of Japan*, *45*, 405–436.

Wells, D. L., & Coppersmith, K. J. (1994, August). New empirical relationships among magnitude, rupture length, rupture width, rupture area, and surface displacement. *Bulletin of the Seismological Society of America*, *84*(4), 974–1002. doi: 10.1785/BSSA0840040974

Yoshida, K., Takagi, R., Fukushima, Y., Ando, R., Ohta, Y., & Hiramatsu, Y. (2024, August). Role of a Hidden Fault in the Early Process of the 2024 M w 7.5 Noto Peninsula Earthquake. *Geophysical Research Letters*, *51*(16), e2024GL110993. doi: 10.1029/2024GL110993

Yoshida, K., Uchida, N., Matsumoto, Y., Orimo, M., Okada, T., Hirahara, S., ... Hino, R. (2023, November). Updip Fluid Flow in the Crust of the Northeastern Noto Peninsula, Japan, Triggered the 2023 M_{w} 6.2 Suzu Earthquake During Swarm Activity. *Geophysical Research Letters*, *50*(21), e2023GL106023. doi: 10.1029/2023GL106023

Yoshikawa, T. (1964). On the Geomorphic Development of Ria Coasts in the Japanese Islands. *The Quaternary Research (Daiyonki-Kenkyu)*, *3*(5), 290–296. doi: 10.4116/jaqua.3.290

Supporting Information for "Earthquake faults recorded in the near-shore bathymetry of Japan's back-arc"

Luca C. Malatesta[1], Shigeru Sueoka[2], Nina-Marie Weiß[1], Boris Gailleton[3], Sumiko Tsukamoto[4,5], Daisuke Ishimura[6,7], Naoya Takahashi[8], Takuya Nishimura[9], Kyoko Kataoka[10], Tetsuya Komatsu[2], Yoshiya Iwasa[11]

[1]Earth Surface Process Modelling, GFZ Helmholtz Centre for Geosciences, Telegrafenberg, 14473 Potsdam, Germany

[2]Tono Geoscience Center, Japan Atomic Energy Agency, 509-5102 Toki, Japan

[3]Geosciences Rennes, University of Rennes, 35042 Rennes, France

[4]LIAG Institute for Applied Geophysics, Stilleweg 2, 30655 Hannover , Germany

[5]Department of Geosciences, University of Tübingen, Schnarrenbergstr. 94-96, 72076 Tübingen, Germany

[6]Department of Geography, Tokyo Metropolitan University, 192-0364 Hachioji, Japan

[7]Department of Earth Sciences, Chiba University, 263-8522 Chiba, Japan

[8]Department of Earth Sciences, Tohoku University, 980-8578 Sendai, Japan

[9]Disaster Prevention Research Institute, Kyoto University, 611-0011 Kyoto, Japan

[10]Research Institute for Natural Hazards and Disaster Recovery, Niigata University, 950-2181 Niigata, Japan

[11]Center for Education and Research of Disaster Risk Reduction and Redesign, Oita University, 870-1192 Oita, Japan

April 17, 2025, 5:50pm

Contents of this file

1. Text S1
2. Figures S1 to S6

Additional Supporting Information (Files uploaded separately)

1. Captions for Dataset S1

Introduction

Text S1. Landscape evolution model

To explore the likelihood of the Noto Peninsula being a transient landscape, we employ a landscape evolution model (Gailleton et al., 2024) to simulate the emergence of an inverted basin and its later tilting (Main text Fig. 3 C, and Fig S5). The simulation does not seek to capture all processes at play, such as ocean waves, sedimentation, and second-order faults (Ota & Hirakawa, 1979). It focuses on the transient response of the fluvial system to the changing tectonics, a fundamental aspect of the landscape. We keep track of the first-order morphology to reasonably compare this simplified model with the complex reality.

We model fluvial erosion using the stream power incision (Howard, 1994) with an implicit finite scheme described by Braun and Willett (2013). The governing equation is as

Corresponding author: L. C. Malatesta, Earth Surface Process Modelling, GFZ Helmholtz Centre for Geosciences, Telegrafenberg, 14473 Potsdam, Germany. (luca.malatesta@gfz.de)

follow:

$$\frac{dz}{dt} = U(x) - K\,A(x)^m \left(\frac{dz}{dx}\right)^n$$

Where z is the elevation [L], x the distance along 1D flow lines following the steepest descent [L], A the drainage area [L^2] and K the erodibility [L^{-2}m+1/T], encompassing rock strength and other local processes. We use $n = 1.11$, matching observations for that drainage area (Ruetenik et al., 2023) and $m = 0.45$. We calibrated $K = 4 \cdot 10^{-5}$ to reproduce the relief and elevation range observed at the field site.

We approximate the peninsula with a 60 by 40 km domain progressively emerging from the sea (Fig. S5). The southern edge is steep to resemble the edge of the Toyama Bay, while the rest of the domain slopes gently to the north. After 750 kyr of uniform rock uplift, a fault breaks in the upper third of the domain and tilts the southern section with 1.5 mm/yr uplift to the north for 250 kyr. The emerging landscape first inherits a strong asymmetry despite the uniform uplift. The larger north-flowing catchments can then cross the newly established zone of faster uplift having already accumulated a large drainage area. This allows the main valleys to keep up with increased rock uplift rate, while the interfluves steepen. Rapidly, the highest topography grows in the north, while the drainage divide remains in the south, a characteristic feature of Noto (Fig. ??B). This period of offset topographic high and drainage divide lasts for ca. 300 kyr under these parameters and ends when the topographic high and the water divide get closer again as the landscape finishes adjusting to the new forcing (Fig. S5 G).

Data Set S1.

ds01.csv: Age, location, and elevation of all the marine terraces from Koike and Machida (2001) used in this article

References

Braun, J., & Willett, S. D. (2013, January). A very efficient O(n), implicit and parallel method to solve the stream power equation governing fluvial incision and landscape evolution. *Geomorphology*, *180–181*(C), 170–179. doi: 10.1016/j.geomorph.2012.10.008

Gailleton, B., Malatesta, L. C., Cordonnier, G., & Braun, J. (2024, January). CHONK 1.0: Landscape evolution framework: Cellular automata meets graph theory. *Geoscientific Model Development*, *17*(1), 71–90. doi: 10.5194/gmd-17-71-2024

Howard, A. D. (1994). A detachment-limited model of drainage basin evolution. *Water Resources \ldots*, *30*(7), 2261–2285. doi: 10.1029/94WR00757

Koike, K., & Machida, H. (2001). *Atlas of Quaternary Marine Terraces in the Japanese Islands.* Tokyo: University of Tokyo Press.

Ota, Y., & Hirakawa, K. (1979). Marine terraces and their deformation in Noto Peninsula, Japan Sea side of Central Japan. *Geographical Review of Japan*, *52*(4), 169–189. doi: 10.4157/grj.52.169

Ruetenik, G. A., Jansen, J. D., Val, P., & Ylä-Mella, L. (2023, September). Optimising global landscape evolution models with 10Be. *Earth Surface Dynamics*, *11*(5), 865–880. doi: 10.5194/esurf-11-865-2023

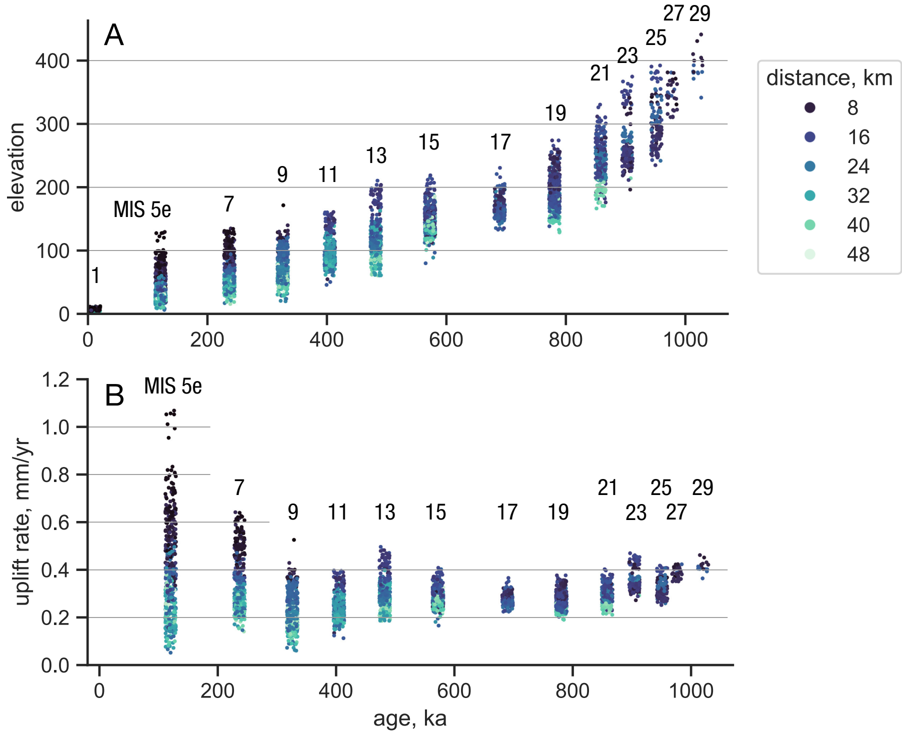

Figure S1. Same data as in Fig. 2. A: marine terrace elevation as a function of age and colored by distance from the reference fault trend. B: respective uplift rates presented in the same manner. The horizontal scatter for each age is only there for visualization purposes.

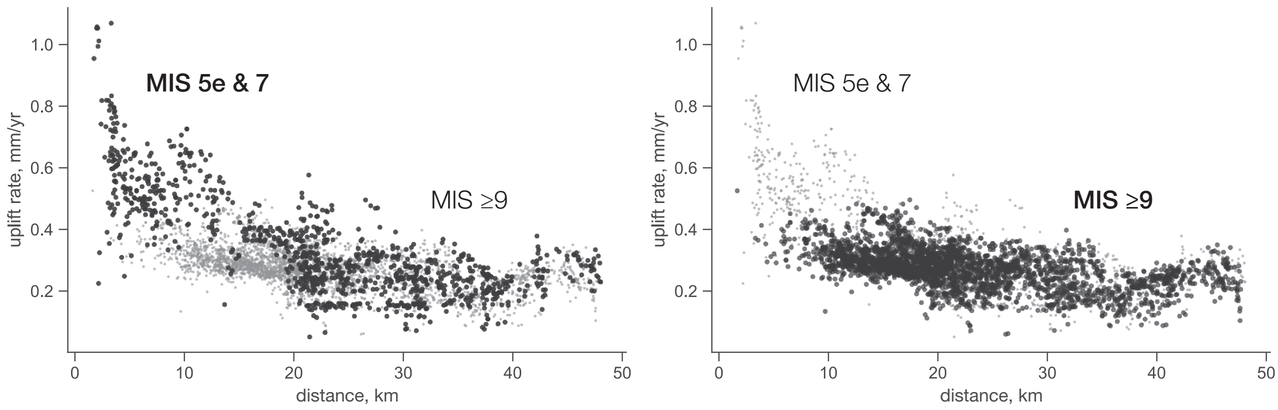

Figure S2. Rate of uplift recorded by marine terraces separating the last two interglacials (MIS 5e and 7) on the left and all terraces of age MIS 9 and older. Same data as Fig. 2 B.

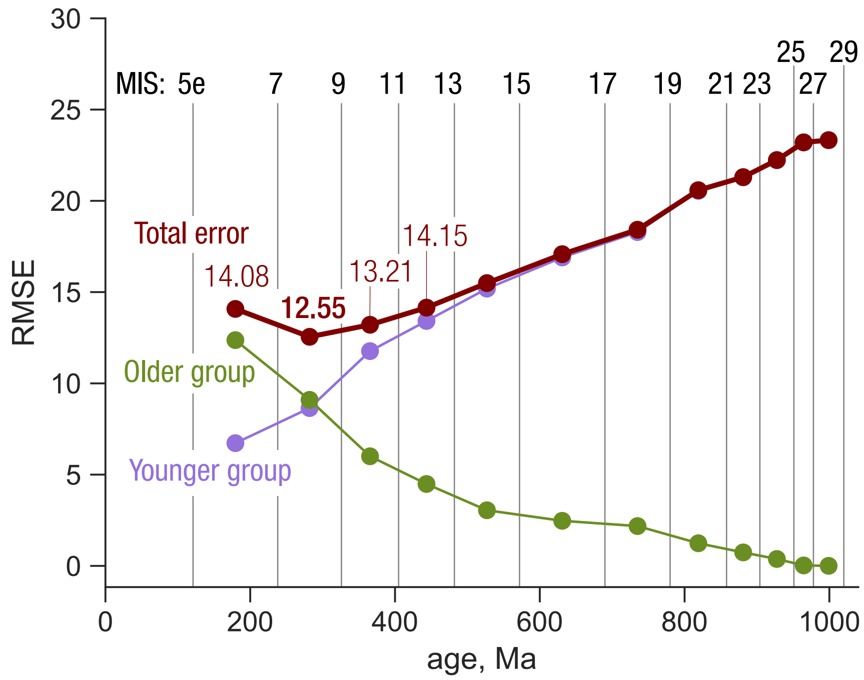

Figure S3. Comparison of the root mean square errors (RMSE) of a second degree regression (Fig. 2 B) using different cutoffs between younger and older terraces. The total error is the square root of the groups' errors squared and combined.

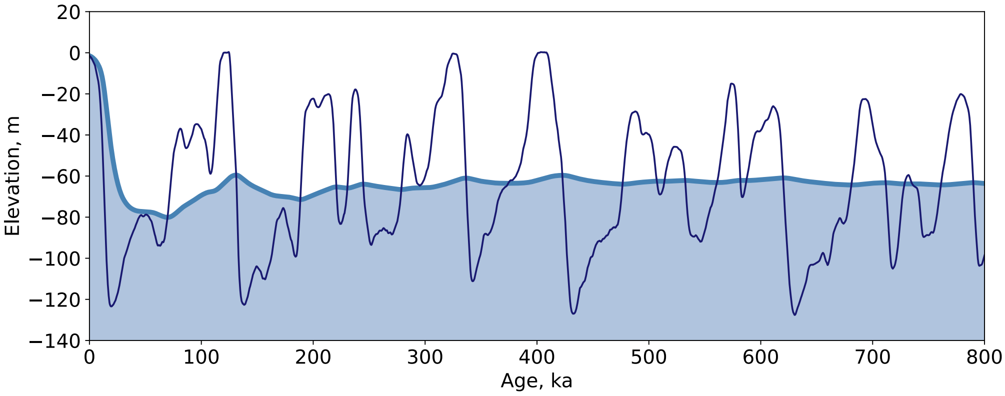

Figure S4. Average sea level over increasingly longer time windows. Sea level curve from Bintanja et al. (2005).

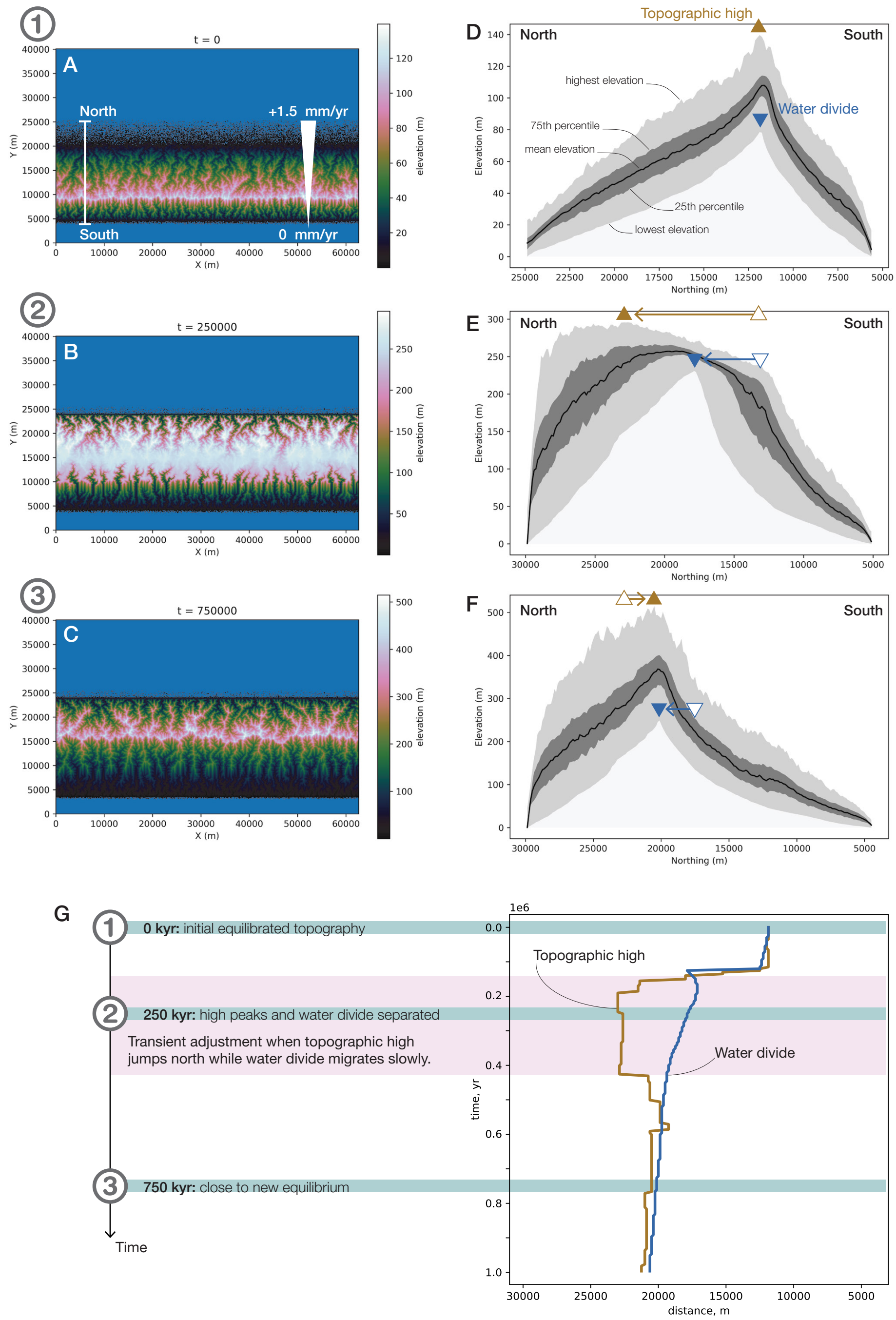

Figure S5. Overview of the landscape evolution model. A to C: Map-view of the landscape responding an uplift gradient faster to the north starting at $t = 0$ from an equilibrated asymmetric ridge inherited from an inverted basin. D to F: North-south swath profiles across the range showing the minimum, maximum, 25th, 75th percentiles, and mean elevations as well as the location of the highest peak and lowest drainage divide. G: Trajectory of topographic high and water divide through time as the model run adjusts to a new uplift field.

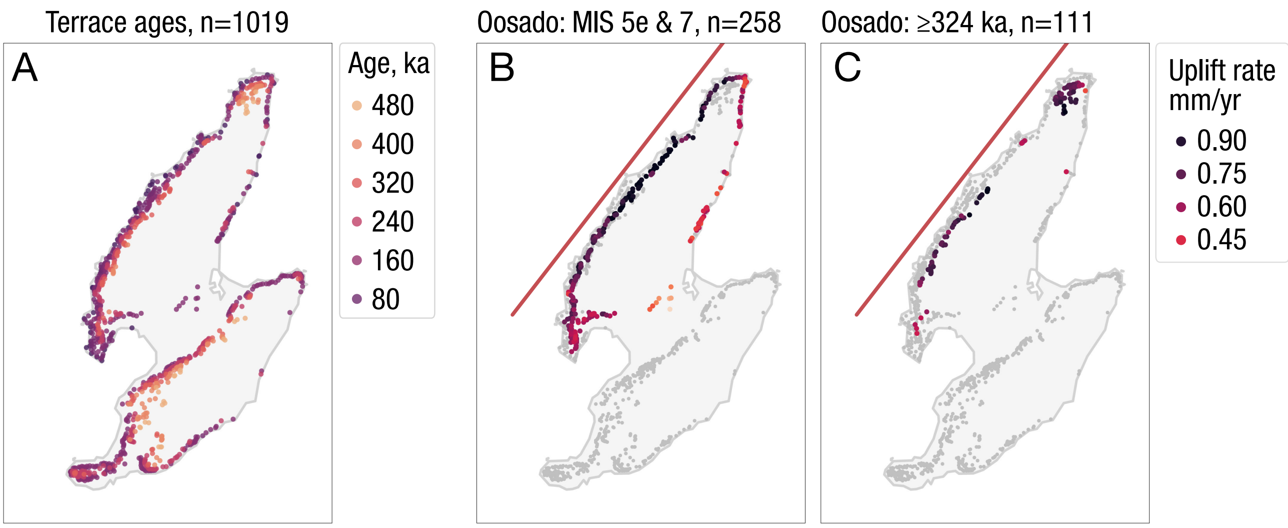

Figure S6. A: age of marine terraces on Sado Island. B: uplift rates derived from the last two interglacial marine terraces in the northern range of Oosado. C: same as B for terraces older than the last two interglacials (MIS 9, 11, and 13).